Toward an Understanding of the Oxidation Process of Methionine Enkephalin: A Combined Electrochemistry, Quantum Chemistry and Quantum Chemical Topology Analysis

Jacqueline Bergès,*[†,‡] Amanda Kamar,[§,∥] Pedro de Oliveira,[§,∥] Julien Pilmé,[†,‡] Eleonora Luppi,[†,‡] and Chantal Houée-Levin[§,∥]

[†]Laboratoire de Chimie Théorique, Sorbonne Universités, UPMC Université Paris 06, UMR 7616 , F-75005 Paris, France
[‡]CNRS UMR 7616, 4 Place Jussieu, 75252 Paris Cedex 5, France
[§]Laboratoire de Chimie Physique, Université Paris-Sud, F-91405 Orsay, France
[∥]CNRS, UMR 8000, F-91405 Orsay, France

ABSTRACT: Recent experimental results about the oxidation of methionine enkephalin by ·OH radicals indicated an intramolecular electron transfer between the C-terminal methionine radical cation and the tyrosine N-terminus too fast to be observed. We have investigated the thermodynamic possibility of this intramolecular electron transfer by calculating the one-electron redox potentials of both residues for several conformations of the peptide, extracted from the experimental data of the Protein Data Bank (1PLW). Using a QM/MM approach, we show that the redox potential of the Met$^{•+}$/Met couple is higher than that of the TyrOH$^{•+}$/TyrOH one (tyrosine is denoted as TyrOH) for all conformations. The intramolecular electron transfer between both residues (from TyrOH to Met$^{•+}$) is thus always thermodynamically allowed. Previously, we had performed topological studies on the intramolecular electron transfer which predicted this charge transfer. A study by cyclic voltammetry pointed out that the wave belonging to methionine is not present when methionine enkephalin is oxidized and only the direct involvement of the tyrosine residue is observed.
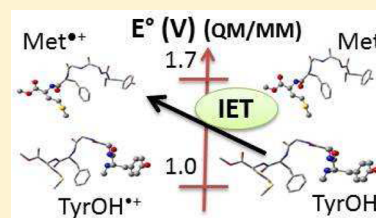
1. INTRODUCTION

Methionine enkephalin (Met-enk) is an opiod pentapeptide (Tyr GlyGlyPhe Met) (Figure 1) whose role is to lower the
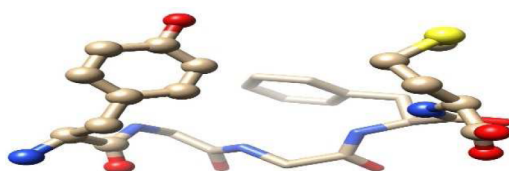

Figure 1. Methionine enkephalin (without the H atoms): the Met and Tyr residues are represented with balls and sticks and the Gly and Phe ones just with sticks.

sensation of pain in inflammation processes.[1−4] The anti-nociceptive action arises from the ability to link to the morphine receptors (μ-receptors) and to the δ-receptors whose importance in management of chronic pain has been recognized.[5]

In the processes occurring during the oxidative stress caused by an inflammation response, Met-enk is subjected to oxidation by reactive oxygen species (ROS) and especially by hydroxyl radicals (·OH). Both tyrosine, essential for the recognition by receptors,[5] and methionine residues are among the main targets of oxidative stress. Methionine is usually considered as a

protective residue against ROS through the formation of methionine sulfoxide.

Because of the importance of the oxidation of this peptide by ·OH radicals *in vivo*, several studies were devoted to its mechanism. Tyrosine one-electron oxidation has been studied by many experimental methods.[6−9] Similarly, the oxidation of methionine has been extensively studied.[10−14] *In vitro* and *in vivo* experiments showed that Met-enk can be oxidized to enkephalin dimers with a dityrosyl bond between the N-terminal tyrosine residues and finally to toxic polymers.[15]

Recently, the one-electron oxidation of Leucine enkephalin (Leu-enk) and Met-enk by ·OH radicals produced by pulse and gamma radiolysis was re-investigated to unveil the mechanisms of degradation of the tyrosine residue.[16,17]

The reaction of ·OH radicals with tyrosine TyrOH in Leu-enk gave the adduct dihydroxyphenylalanine, with an additional hydroxyl group on the phenyl cycle in *ortho*- or *meta*-position, while in Met-enk the tyrosyl radical was the major transient. (For the sake of clarity, we adopted a special denomination for the tyrosine residue: TyrOH instead of Tyr, because of the importance of the reactions involving the hydroxyl group.) In agreement with these results, the major compound was the dimer linked by dityrosines.[18] This was interpreted as coming

from a fast Intramolecular (sub-nanosecond) one-Electron Transfer (IET) from the tyrosine residue TyrOH to the methionine radical cation Met$^{\bullet+}$ (Reaction 1), followed by a deprotonation of the tyrosyl radical cation TyrOH$^{\bullet+}$ (Reaction 2) to the tyrosyl radical TyrO$^{\bullet}$ due to the very low pK_a of TyrOH$^{\bullet+}$ ($\leq$1). Both steps are too fast to be observed by pulse radiolysis but are consistent with the final products of oxidation.[18]
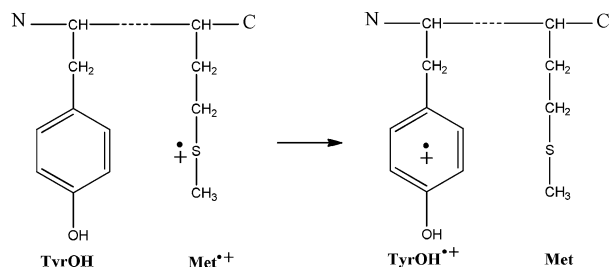
Reaction (1) The proposed Intramolecular Electron Transfer from tyrosine TyrOH to the methionine radical cation Met$^{\bullet+}$, leading to the tyrosyl radical cation TyrOH$^{\bullet+}$.
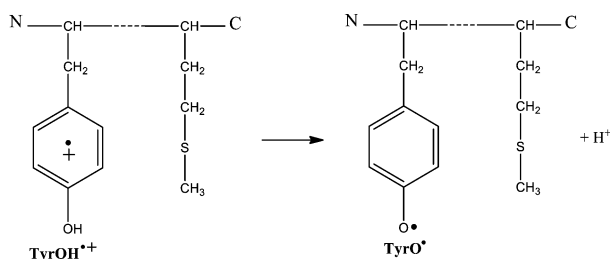

Reaction (2) Formation of the tyrosyl radical TyrO$^{\bullet}$ by deprotonation of the tyrosyl radical cation TyrOH$^{\bullet+}$.

Reaction 1 is the result of the combination of two half-reactions, which are Reaction 3 and the reverse of Reaction 4:

$$Met^{\bullet+} + e^- \rightarrow Met \tag{3}$$

$$TyrOH^{\bullet+} + e^- \rightarrow TyrOH \tag{4}$$

It should be noted that, experimentally, one has access just to the combination of oxidation and proton loss taken together, because the pK_a of TyrOH$^{\bullet+}$ is low ($\leq$1) and the proton transfer reaction is very fast:
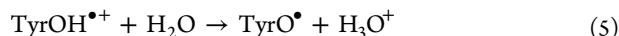
$$TyrOH^{\bullet+} + H_2O \rightarrow TyrO^{\bullet} + H_3O^+ \tag{5}$$

Hence, the observed redox couple is (TyrO$^{\bullet}$ + H$_3$O$^+$)/(TyrOH + H$_2$O), corresponding to the overall process given by Reaction 6, which is obtained by combining the reverse of Reaction 4 with Reaction 5:

$$TyrOH + H_2O \rightarrow TyrO^{\bullet} + e^- + H_3O^+ \tag{6}$$
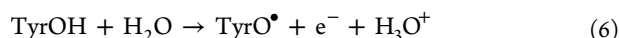
Nevertheless, with computations we are able to mimic roughly this redox reaction by decomposing the whole process into two steps corresponding to an electron transfer plus a deprotonation reaction.

We have performed preliminary theoretical approaches of the oxidation competition between TyrOH and Met in isolated peptide models.[19,20] These first thermodynamic data indicated that TyrOH$^{\bullet+}$ was more stable than Met$^{\bullet+}$.

The purpose of this work is to enlarge the preceding studies to this process, which takes place in Met-enk. In order to test the thermodynamic feasibility of intramolecular proton-coupled electron transfer (PCET) in this peptide, we evaluated the redox potentials of each couple involved, i.e., Met$^{\bullet+}$/Met and TyrOH$^{\bullet+}$/TyrOH, as well as the deprotonation energy of (TyrO$^{\bullet}$ + H$^+$)/TyrOH$^{\bullet+}$.

Experimental NMR conformations of this peptide in micelles were published in the Protein Data Bank (1PLW in PDB).[21] Many conformational studies were performed using molecular dynamics (MD) and Monte Carlo (MC) simulations[22−25] including implicit or explicit solvent. In agreement with the experimental results, a great flexibility of the pentapeptide was observed. The predominant geometries pointed out by Replica MD in explicit aqueous solution[24] could be divided into two groups: helicoidal (one or several α-helix substructures) and nonhelicoidal (β-hairpin and U-shaped structures), where the residues could be linked by different H bonds. By increasing the temperature, the swap from one conformation to another along the dynamics time is easy because of the low energy barrier between them. In some of them, the peptidic chain was folded so that Met and Tyr residues could be as close as 4 Å from each other, whereas in others it was extended and these residues were 12 Å apart. It was thus of interest to explore the thermodynamic possibilities of IET in conformation samples as a function of the local geometry.

Recently, two studies of the IET in polypeptides and of Metenk50 were performed by DFT and MD methods.[25,26] In the first one, various mechanisms of IET between TyrO$^{\bullet}$ and cysteine (Cys) separated by several alanine residues (1−4) in water have been investigated using the Marcus theory.[25] For this peptide, the mechanism consists of a PCET involving a proton exchange between the −OH group of TyrOH and the −S$^{\bullet}$ group of the Cys radical. In the second one,[26] dealing with Met-enk, the IET, that is Reaction 1, took place between two diabatic states, [Met$^{\bullet+}$···TyrOH] and [Met···TyrOH$^{\bullet+}$] in the most folded conformation, which is peculiar. In this paper, we re-examine these results in the light of the thermodynamic data. In addition, the theoretical study was completed by an approach by cyclic voltammetry as a function of the pH.

2. EXPERIMENTAL SECTION

Computational Methodology. The computations were performed thanks to the Gaussian G09 package[27] using the QM/MM method (Oniom). The Quantum Mechanics (QM) method chosen was the DFT method pbe0/6-31G(d), which is an appropriate method for redox potential calculations, as it was shown in our previous paper.[28] For the Molecular Mechanics (MM) method, we used the empirical potentials uff with the electrostatic charges embedded (Qeq). The solvation effects (water) were accounted for with the COSMO option for the Polarized Continuum Model CPCM.

The peptide underwent the QM/MM partitions depicted in Figure 2. Briefly, in the first one, Met was in the QM part of Met-enk (Figure 2, left). In the second one, TyrOH was in the QM part of Met-enk (Figure 2, right).

Gibbs Energies. For each pentapeptide conformation, the Gibbs energies $\Delta G^{\circ}(R)$ and $\Delta G^{\circ}(R^{\bullet+})$ of the molecule and cation species (R being either Met or TyrOH), respectively, were calculated. ΔG°_3 and ΔG°_4 are the Gibbs free energies of reduction of R$^{\bullet+}$ into R, corresponding to Reactions 3 and 4, both being equal to $\Delta G^{\circ}(R) - \Delta G^{\circ}(R^{\bullet+})$.
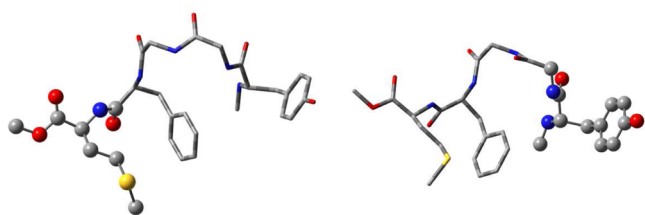
Figure 2. QM parts of Met-enk are represented by "ball and sticks". Left: Met; right: TyrOH.

The Gibbs free energy $\Delta G°_5$ concerns the deprotonation of TyrOH$^{•+}$ (Reaction 5).

Redox Potentials. The one-electron redox potentials were calculated as described in ref 29. Briefly, the standard redox potential of a peptide R$^{•+}$/R couple relative to the normal hydrogen electrode (NHE), $E°(R^{•+}/R)$, is defined by eq 7

$$E°(R^{•+}/R) = -(\Delta G°_{3\ or\ 4} - \Delta G°(aq)NHE)/F \qquad (7)$$

where F is the Faraday constant ($F = 96\,485$ C mol^{-1}) and $\Delta G°(aq)NHE$ is the Gibbs free energy change for the standard hydrogen half-cell reaction:[30]

$$H^+(aq) + e^- \rightarrow \frac{1}{2}H_2(g)$$
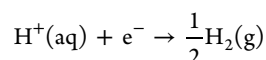
$$(\Delta G°(aq)NHE = -418\ kJ\ mol^{-1}\ (ignoring\ the\ electron))$$

The N-and C-terminals, which should be charged in the zwitterionic form, were methylated in order to avoid artifacts.[27]

Topological Analysis by TD-RHO and TD-ELF Functions. The quantum chemical topology tools were used for monitoring the dynamics associated with the tunneling of an electron between the donor and the acceptor. The topological analysis of the stationary density functions is well-known,[31] namely the electron density, Quantum Theory of Atoms In Molecules (QTAIM) approach,[32] where only atomic populations are obtained and the Electron Localization Function (ELF) of Becke and Edgecombe,[33,34] where bonding and nonbonding populations can be analyzed in more detail. Indeed, we have recently proposed to extend the topological analysis of these functions in a time-dependent context (TD-RHO and TD-ELF).[26] We have also shown how these functions can be calculated in the framework of the constrained density functional theory[35] and upon applying the theory of gradient dynamical systems.[31] Interestingly, the coupled TD-ELF/TD-RHO analysis appears as a suitable way to rationalize the evolution of the electronic structure during an IET between a donor and an acceptor.

Electrochemistry. A one-compartment cell with a standard three-electrode configuration was used for cyclic voltammetry experiments, which were carried out with an EG&G PAR 273A potentiostat computer-controlled via the M270 software. The reference electrode was a saturated calomel electrode (SCE), the counter electrode a platinum gauze of large surface area, and the working electrode a glassy carbon disk. The buffers used were prepared with pure water obtained from a Milli-Q Integral 5 purification set (water resistivity: 18.2 MΩ·cm) and were the following: 0.2 M Li$_2$SO$_4$/H$_2$SO$_4$, pH = 1.00; 0.2 M Li$_2$SO$_4$/H$_2$SO$_4$, pH = 2.00; 0.2 M Li$_2$SO$_4$/H$_2$SO$_4$, pH = 3.00; 1.0 M LiCH$_3$COO/CH$_3$COOH, pH = 4.00; 0.4 M LiCH$_3$COO/CH$_3$COOH, pH = 5.00; 0.4 M Na$_2$HPO$_4$/NaH$_2$PO$_4$, pH = 6.00; 0.4 M NaH$_2$PO$_4$ 0.4 M/NaOH, pH = 7.00. Solutions were made with Met-enk (Bachem), Met (Sigma-Aldrich), and TyrOH (Sigma-Aldrich) used as received from the suppliers. All solutions had a concentration of 1.0 mM and were thoroughly deoxygenated with argon prior to the cyclic voltammetry experiments.

3. RESULTS

Theoretical Results. As starting points, we have selected, among the ca. 80 experimental conformations in the PDB, 8 conformations named "metenkX" (with X = 10, 20, 30, ...80) according to their number in the PDB file, and we have fully optimized them in the molecular and in the radical states. For some cations, we happened to encounter convergence difficulties. Thus, we used as starting points the optimized conformation of the molecule.

Gibbs Free Energies of the Various Cations with Different QM/MM Partitions. The Gibbs free energies of the different molecules and radicals, together with the d_{S-O} distances between Met and TyrOH and the d_{S-C} distances

Table 1. Gibbs Free Energies (in Atomic Units), d_{S-O} Distances between Met and TyrOH, and d_{S-C} Distances between Met and Phe (the Shortest Ones) in the Optimized Structures[a]

	molecule	cation		molecule	cation	
	metenk10			metenk20		
$\Delta G°$ + 990 (a.u.)	−0.95074	−0.72357		−0.88744	−0.67075	
d_{S-O} (Å)	5.63	5.21	I	10.91	11.30	I
d_{S-C} (Å)	6.48	7.80		4.54	4.08	
	metenk30			metenk40		
$\Delta G°$ + 990 (a.u.)	−0.9186	−0.70746		−0.94252	−0.71718	
d_{S-O} (Å)	5.85	5.71	I	4.62	4.53	F
d_{S-C} (Å)	3.74	3.88		5.25	4.48	
	metenk50			metenk60		
$\Delta G°$ + 990 (a.u.)	−0.95145	−0.72315		−0.8897	−0.67171	
d_{S-O} (Å)	4.95	4.23	F	8.32	9.94	E
d_{S-C} (Å)	3.69	3.84		4.62	5.64	
	metenk70			metenk80		
$\Delta G°$ + 990 (a.u.)	−0.91662	−0.68625		−0.95460	−0.73959	
d_{S-O} (Å)	4.14	4.83	F	8.75	9.10	E
d_{S-C} (Å)	4.66	4.93		5.63	5.47	

[a]Calculations ONIOM(pbe0/6/31G(d):uff = Qeq) plus solvation (CPCM). QM part: Met.

Table 2. Gibbs Free Energies (in Atomic Units), d_{S-O} Distances between Met and TyrOH, and d_{S-C} Distances between Met and Phe (the Shortest Ones) in the Optimized Structures[a]

	molecule	cation	neutral		molecule	cation	neutral	
		metenk10				metenk20		
$\Delta G° + 686$ (a.u.)	−1.24739	−1.04875	−0.62194		−1.28886	−1.08229	−0.66567	
d_{S-O} (Å)	6.37	6.32	7.10	I	6.94	7.20	6.81	I
d_{S-C} (Å)	6.79	6.93	6.71		4.13	3.91	3.97	
		metenk30				metenk40		
$\Delta G° + 686$ (a.u.)	−1.26466	−1.05363	−0.64595		−1.27747	−1.06640	−0.65637	
d_{S-O} (Å)	6.20	5.22	6.24	I	9.24	9.00	9.26	I
d_{S-C} (Å)	3.99	3.76	3.91		4.97	4.94	4.94	
		metenk50				metenk60		
$\Delta G° + 686$ (a.u.)	−1.27188	−1.07249	−0.65374		−1.24713	−1.05152	−0.62632	
d_{S-O} (Å)	5.10	5.12	4.94	F	5.99	5.43	6.14	I
d_{S-C} (Å)	3.67	3.60	3.61		4.91	4.90	4.85	
		metenk70				metenk80		
$\Delta G° + 686$ (a.u.)	−1.27306	−1.07156	−0.64657		−1.29693	−1.09118	−0.65267	
d_{S-O} (Å)	6.35	7.58	6.41	I	12.16	10.77	9.78	E
d_{S-C} (Å)	5.67	6.02	5.69		6.23	5.67	5.60	

[a]Calculations ONIOM (pbe0/6/31G(d):uff = Qeq) plus solvation (CPCM). QM part: TyrOH.
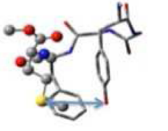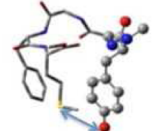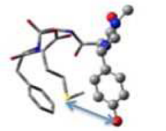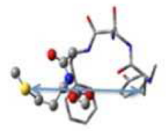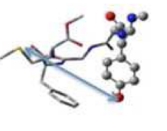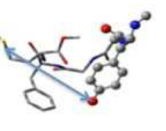
between Met and Phe (the shortest ones), are summarized in Tables 1 and 2. These two distances were used as markers of the folding of the peptide. Three major kinds of structures can be identified: the folded ones (for d_{S-O} and d_{S-C} < 5.0 Å: F in Tables 1 and 2), the extended ones (for d_{S-O} > 8.0 Å and d_{S-C} > 6.0 Å: E in Tables 1 and 2), and the others being the intermediate ones (I in Tables 1 and 2).

It appeared that, in both tables, metenk50 has the most folded conformation with TyrOH, Phe and Met very close to each other and metenk80 is the most extended one where TyrOH and Met can be very far from each other (ca. 12 Å).

As it could be expected, the optimized conformations of the neutral tyrosyl radical and tyrosine residue (TyrO· and TyrOH, respectively) exhibit only slight differences from each other (see Table 2 for examples). The conclusions are somewhat different for the radical cations Met$^{•+}$ or TyrOH$^{•+}$, depending on the electrostatic interactions between the charged residue and the remaining atoms of the peptide. The distances between Met$^{•+}$ and TyrOH (Table 1) were different from those in the molecules: shorter for metenk10 and 50 and longer for metenk20, 60, 70 and 80. The trend can be different when considering the TyrOH ionizations (Table 2). The distances between TyrOH$^{•+}$ and Met are shortened (metenk30 and 80), practically unchanged (metenk50) or lengthened for metenk20 and 70, as observed for Met$^{•+}$ radical cations (Table 1). Some examples of the optimized geometries are shown in Table 3. When Met$^{•+}$ is in the QM part, the spin density is fully localized on the sulfur atom ($\rho S \approx 0.90$). In TyrOH$^{•+}$, it is delocalized on the oxygen atom and on the aromatic cycle, or even on the terminal nitrogen atom. However, in the molecular state as well as in the radical cations, the most stable conformation is metenk80. The lowest Gibbs free energy of this conformation was thus taken as the reference. In Figure 3 are displayed the relative Gibbs free energy differences defined for the molecular conformations as $\Delta G°(mol) = \Delta G°X(mol) - \Delta G°80(mol)$, likewise for the cations ($\Delta G°(cat) = \Delta G°X(cat) - \Delta G°80(mol)$).

The analysis of Figure 3 reveals several general trends with respect to metenk80 as reference. As far as the molecules are concerned, and irrespective of the QM part, metenk60 is higher in energy by ca. 140−170 kJ mol^{-1} and metenk50 by ca. 10−60

Table 3. Optimized Radicals from Two Different Met-enk Structures, metenk50 (Folded) and metenk80 (Extended) with Their Distances d_{S-O}[a]

Cation Met$^{•+}$	Cation TyrOH$^{•+}$	Neutral radical TyrO$^{•}$
	MetEnk 50	
	MetEnk80	

[a]QM/MM calculations: high level with Met in the QM part (left column); high level with TyrOH in the QM part (center and right columns).

kJ mol^{-1}. A similar behavior is also observed for the radical cations, $\Delta G°(cat)$ being higher by 200 kJ mol^{-1} for metenk60 and by only 50 kJ mol^{-1} for metenk50.

In Table 4 are summarized the Gibbs free energies of Reactions 3 and 4 in kJ mol^{-1}, corresponding to the one-electron reduction of Met$^{•+}$ ($\Delta G°_3$) and of TyrOH$^{•+}$ ($\Delta G°_4$), and those of Reaction 5. The association of the reverse of Reaction 4 with Reaction 5 corresponds to the sequence of an electron transfer (oxidation) plus deprotonation (PCET), and thus to the homolytic dissociation of the OH bond in TyrOH. When the deprotonation of the latter is taken into account in the calculations, even relatively roughly, the redox potentials are lowered and the driving force of the electron transfer between Met$^{•+}$ and TyrOH increases. Indeed, the Gibbs free energy $-\Delta G°_4 + \Delta G°_5$ is much lower than the one corresponding to the ionization of Met ($-\Delta G°_3$).

Redox Potentials of Both Couples Met$^{•+}$/Met and TyrOH$^{•+}$/TyrOH. The redox potentials of both couples Met$^{•+}$/
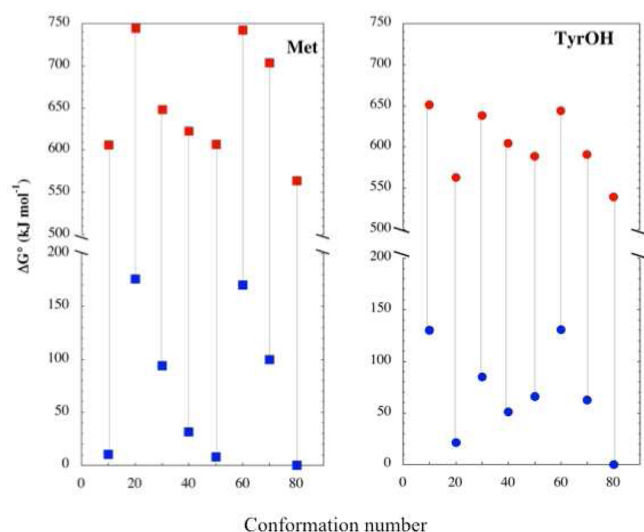
Figure 3. Gibbs free energies (in kJ mol^{-1}) of the molecules $\Delta G°$(mol) and radical cations $\Delta G°$(cat) for the selected geometries 10−80. The reference is the conformation of lowest energy, i.e., metenk80 in both cases. On the lowest part of these diagrams are represented (in blue) the $\Delta G°$(mol) values and on the highest part (in red), the $\Delta G°$(cat). Left, squares: **Met** in the QM part; right, circles: **TyrOH** in the QM part.

Table 4. Gibbs Free Energies of Reduction of R$^{•+}$ into R, $\Delta G°_3$ and $\Delta G°_4$, and of Deprotonation of TyrOH$^{•+}$, $\Delta G°_5$, in kJ mol^{-1}^{a}

	Met	TyrOH		
Met-enk	$-\Delta G°_3$	$-\Delta G°_4$	$\Delta G°_5$	$-\Delta G°_4 + \Delta G°_5$
10	595.86	521.02	−169.31	351.71
20	568.37	535.79	−140.77	395.02
30	553.89	553.52	−119.13	434.39
40	591.06	553.63	−125.30	428.33
50	598.82	522.99	−148.17	374.82
60	571.93	513.08	−165.09	347.99
70	604.25	528.52	−164.54	363.98
80	563.96	539.67	−200.00	339.67

^{a}The QM part is Met (Reaction 3) or TyrOH (Reaction 4).

Met and TyrOH$^{•+}$/TyrOH are displayed in Table 5 and in Figure 4.

The redox potential of Met varies between 1.4 and 1.9 V vs NHE, whereas that of the TyrOH moiety varies between 1.0 and 1.4 V. When the deprotonation is taken into account, as it

Table 5. Redox Potentials $E°$ (in V vs NHE) for Each Partition of the QM/MM Calculations^a

Met-enk	$E°_{Met}$ (V)	$E°_{TyrOH}$ (V)	$\Delta E°$ (V)
10	1.84	1.07	0.77
20	1.56	1.22	0.34
30	1.41	1.40	0.01
40	1.79	1.41	0.38
50	1.87	1.09	0.78
60	1.60	0.99	0.61
70	1.93	1.15	0.78
80	1.51	1.26	0.25

^{a}The QM part is either Met or TyrOH. The driving force is defined as the difference $\Delta E° = E°_{Met} - E°_{TyrOH}$.

was roughly estimated ($-\Delta G°_4 + \Delta G°_5$, Table 4), the Gibbs free energies are drastically lower and the redox potentials as well.

As for the driving force of the IET (defined as $\Delta E° = E°_{Met} - E°_{TyrOH}$), it varies from 0 to 0.8 V, but it is always positive (Table 5, Figure 4), showing that the IET from TyrOH to Met$^{•+}$ is always thermodynamically feasible whatever the geometry of the peptide. The highest driving forces (ca. 0.8 V for metenk10, 50 and 70) do not belong to the most stable geometry ($\Delta E° = 0.25$ V for metenk80), and they correspond to $d_{S−O}$ distances varying between 5 and 7 Å. The lowest value, close to 0 V, corresponds to a close proximity of both residues (5.5−6 Å). From a thermodynamic point of view, there is no correlation between the driving force and the conformation of the peptide.

Topological Analyses. The electron transfer was recently monitored by means of the topological analysis of time-depending density functions[26] TD-RHO and TD-ELF. These analyses were performed in the context of the constrained DFT using the two-state approximation coded in a local version of the program deMon2k.[36] Interestingly, this study has shed light on the intramolecular reorganization of the density during the IET process. We have considered only one conformation, metenk50, where the small distance between Met and TyrOH could facilitate the determination of the electron pathways. Here, the TD-RHO and TD-ELF populations have been found useful to understand the evolution of the electronic structure along the IET process, by precisely indicating which bonds and lone pairs are involved in it. However, the IET was seen as reversible and symmetric, because of lack of thermodynamics considerations.

The ELF topology analysis indicates that the IET process is not associated with dramatic changes in the electronic structure of the molecule such as broken covalent bonds. However, QTAIM charges generally vary during the IET process, especially for the sulfur atom. Indeed, Figure 5 (left) displays the relative QTAIM charges of all the atoms, with respect to the initial charges, as a function of time during the half period of the IET process (16 ps). Interestingly, this picture clearly shows a strong increase of the sulfur charge (+0.42 electrons, Figure 5, right) between the initial diabatic state [TyrOH,Met$^{•+}$] and the final one [TyrOH$^{•+}$,Met]. In addition, the ELF population analysis reveals that this increase is precisely localized around the lone pairs of the sulfur atom and less in the regions binding the sulfur to the carbons of Met.

Electrochemistry. Met-enk is irreversibly oxidized on the surface of a glassy carbon electrode in a 0.4 M NaH$_2$PO$_4$/NaOH, pH = 7.00 buffer (Figure 6). When scanning at 10 mV s^{-1}, the anodic peak potential falls at E_{pa} = 0.758 V vs SCE (E_{pa} = 1.000 V vs NHE), the wave onset potential being at E_{onset} = 0.520 V vs SCE (E_{onset} = 0.762 V vs NHE). This behavior is very similar to that exhibited by TyrOH, which is also irreversibly oxidized under the same experimental conditions at E_{pa} = 0.798 V vs SCE (E_{pa} = 1.040 V vs NHE), with the wave onset at E_{onset} = 0.578 V vs SCE (E_{onset} = 0.820 V vs NHE). Met is irreversibly oxidized as well, but at a much higher potential: E_{pa} = 1.502 V vs SCE (E_{pa} = 1.744 V vs NHE), with the wave onset at E_{onset} = 1.324 V vs SCE (E_{onset} = 1.566 V vs NHE). The cyclic voltammetry results for the oxidation of Met-enk indicate that just the TyrOH residue (and not the Met one) responds within the potential range applied to the working electrode.
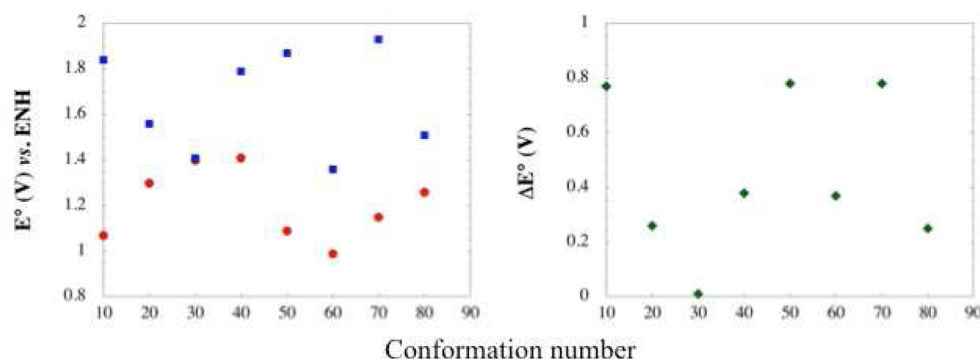
Figure 4. Left: the redox potentials $E°$ (in V vs NHE) of the TyrOH$^{•+}$/TyrOH couple (red dots) and of the Met$^{•+}$/Met couple (blue squares) for the selected geometries (metenk10 to 80). Right: the driving force $\Delta E°$ (in V) of the IET for each conformation.
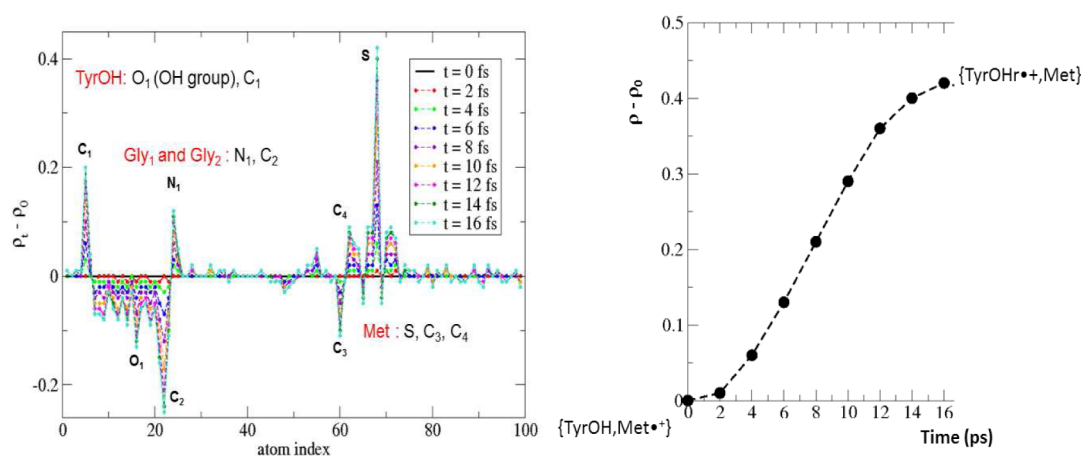

Figure 5. Relative QTAIM charges as a function of time with respect to the initial charges during the half period of the IET process (16 ps). Left: all the atoms. Right: S atom.
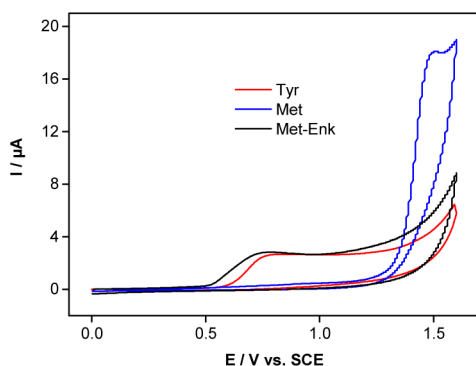

Figure 6. Cyclic voltammograms of 1.0 mM Met-enk, Met and Tyr in 0.4 M NaH$_2$PO$_4$/NaOH, pH = 7.00 buffer, at 10 mV s^{-1}.

As expected from Reactions 4 and 5, the oxidation of Met-enk depends on the pH of the medium, which means that protons are implicated in the redox mechanism. This peptide becomes easier to oxidize as the pH is increased from 1.00 to 7.00 (Figures 6 and 7). The oxidation process exhibits two successive waves, which may be due to different conformations of the pentapeptide. These waves are clearly separated at lower pH values (Figure 7A), but the lower potential wave becomes less noticeable as the pH increases (Figure 7B) and hardly observable above pH 5.00 (Figure 7C). The plot of oxidation peak potentials, E_{pa}, as a function of the pH of the medium for these two waves gives straight lines with slopes very close to −60 mV/pH (Figure 8), implying the involvement of a proton (H$^+$) for each electron transferred. This outcome is in very good agreement with the Nernst eq 8 associated with Reaction 6, assuming that E_{pa} behaves the same way as the potential given by the Nernst equation:

$$E = E° + 0.06 \log \frac{[\text{TyrO}^{•}]}{[\text{TyrOH}]} - 0.06\text{pH} \tag{8}$$

This also confirms that the pK_a for the TyrOH$^{•+}$/TyrO$^{•}$ couple is lower than 1. Indeed, for Reaction 4, the corresponding Nernst eq 9 is

$$E = E° + 0.06 \log \frac{[\text{TyrOH}^{•+}]}{[\text{TyrOH}]} \tag{9}$$

where the redox potential is independent of the pH. Therefore, a straight line parallel to the x axis should have been obtained for pH values lower than the pK_a, but as no such behavior was observed within the pH range studied ($1.00 \leq \text{pH} \leq 7.00$), the p$K_a$ is necessarily lower than 1.

Under the present experimental conditions, the anodic peak potential, E_{pa}, is related to the redox potential, $E°$, by the following eq 10[37]

$$E_{pa} = E° - 0.9\left(\frac{RT}{nF}\right) + \frac{RT}{3nF} \ln \frac{2kCRT}{3nFv} \tag{10}$$

where C is the bulk concentration, v the scan rate and k the rate constant for a homogeneous chemical reaction. Equation 10 allowed $E°$ to be estimated at 1.4 V vs NHE at pH = 0. This
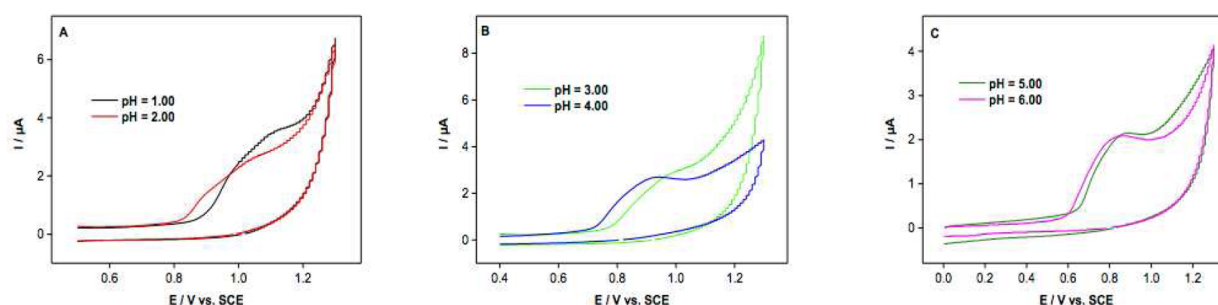
Figure 7. Cyclic voltammograms of 1.0 mM Met-Enk obtained at 10 mV s^{-1} in several buffers having different pHs: (A) 1.00 and 2.00; (B) 3.00 and 4.00; (C) 5.00 and 6.00.
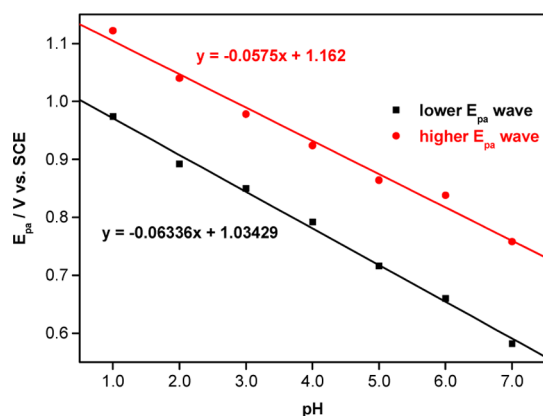

Figure 8. Dependence of the anodic peak potential, E_{pa}, on the pH for the two-oxidation waves of Met-enk.

result is in good agreement with the values arrived at by the theoretical calculations previously shown in this work.

4. DISCUSSION AND CONCLUSION

In the oxidation of the pentapeptide Met-enk by ·OH radicals, experimental results in gamma and pulse radiolysis showed that the main targets were both Met and TyrOH residues. For Met-enk, TyrO$^{•}$ was the major transient, instead of the radical adduct which would appear during the direct reaction of ·OH radicals with TyrOH. In agreement with these results, the major final compound was the dimer linked by dityrosines.[18] The electrochemistry experiments (this work) like the pulse radiolysis ones,[17] revealed that the Met oxidation is not detected, only the involvement of the TyrOH residue in the oxidation being observed. These results were interpreted as coming from a fast intramolecular (sub-nanosecond) one-electron transfer from the TyrOH residue to Met$^{•+}$.

Our present aim was to follow a thermodynamic approach of the IET by calculating the redox potential for the TyrOH$^{•+}$/TyrOH and Met$^{•+}$/Met couples. Because of the great flexibility of the pentapeptide, several starting points taken from the PDB structures (extended, folded and intermediate) were considered. Geometry optimizations were performed for the molecules and for the derived radicals, neutral as well as charged, using the methodology of QM/MM. This calculation strategy allows one to differentiate the localizations of the oxidation by assaying two types of QM partitions, with either TyrOH or Met being in the QM part (Figure 2). If optimized geometries of the molecules and of the neutral radical are close to each other, the Met-enk geometries are more modified when Met or TyrOH are positively charged.

Comparison of the Gibbs energies of the molecular and radical species for various geometries (Figure 3) indicates that the stabilities of the various conformations are not directly connected to the folding of the pentapeptide, the latter being characterized by the distances between TyrOH and Met. Nevertheless, the most elongated conformation (metenk80) remains the most stable one even after ionization. Recently, we have computed the one-electron redox potential of the Met residue in dipeptides and found that it could vary importantly (1−2 V vs NHE) with the geometry of the peptide.[28] Likewise, the redox potential for Met-enk varies in a narrower range (between 1.4 and 1.9 V vs NHE, Table 5) using the same methods of computation. Nevertheless, the redox potential is always higher than that of the TyrOH residue.

The tyrosyl radical TyrOH$^{•+}$ is very acidic, as confirmed by electrochemistry, its pK_a being lower than 1. Hence, for pH > 1, this species is deprotonated (TyrO$^{•}$) and electron transfer involving TyrOH is always coupled to proton transfer. For the amino acid and for dipeptides, previous measurements of $E°$(TyrO$^{•}$ + H$^+$/TyrOH) gave 0.85−0.94 V vs NHE at pH 7.[37−40] Interestingly, the experimental value in Met-enk (1.05 V) is higher by more than 0.1 V, which may be rationalized by environmental effects.

The driving force of the electron transfer between TyrOH and Met$^{•+}$ is always positive (Table 5 and Figure 4) and is even enhanced by the deprotonation (estimated in Table 4), which means that the IET is thermodynamically irreversible. Therefore, in this context, the QTAIM charges provide a characterization of the electronic structure for each time point, as shown in Figure 5. During the irreversible process, the major change is the increase of the sulfur charge as a function of time from 15.58 electrons ($t = 0$ ps, with [TyrOH,Met$^{•+}$]) to 16 electrons ($t = 16$ ps, with [TyrOH$^{•+}$,Met]) (Figure 5, right), and a concomitant decrease of the tyrosine atom charges.

In conclusion, the combination of experimental electrochemical measurements (cyclic voltammetry), quantum chemistry and quantum chemical topology analyses sheds light on the initial, not detectable, participation of the methionine residue in the oxidation of Met-enk. The radical cation TyrOH$^{•+}$ is formed by fast IET and undergoes deprotonation.

■ AUTHOR INFORMATION

Notes
The authors declare no competing financial interest.

■ ACKNOWLEDGMENTS

■ ABBREVIATIONS

Cys, cysteine; Gly, glycine; IET, intramolecular electron transfer; Met, methionine; Met-enk, methionine enkephalin; PCET, proton-coupled electron transfer; Phe, phenylalanine; ROS, reactive oxygen species; Tyr, tyrosine

■ REFERENCES

(1) Machelska, H. Targeting of Opioid-Producing Leukocytes for Pain Control. *Neuropeptides* **2007**, *41*, 355−363.

(2) Henry, B.; Duty, S.; Fox, S. H.; Crossman, A. R.; Brotchie, J. M. Increased Striatal pre-Proenkephalin B Expression is Associated with Dyskinesia in Parkinson's Disease. *Exp. Neurol.* **2003**, *183*, 458−468.

(3) Thanavala, V.; Kadam, V. J.; Ghosh, R. Enkephalinase Inhibitors: Potential Agents for the Management of Pain. *Curr. Drug Targets* **2008**, *9*, 887−894.

(4) Smith, H. S. Peripherally-Acting Opioids. *Pain Physician* **2008**, *11*, S121−S132.

(5) Terenius, L.; Wahlstrom, A.; Lindeberg, G.; Karlsson, S.; Ragnarsson, U. Opiate Receptor Affinity of Peptides Related to Leu-Enkephalin. *Biochem. Biophys. Res. Commun.* **1976**, *71*, 175−179.

(6) Hoganson, C. W.; Tommos, C. The Function and Characteristics of Tyrosyl Radical Cofactors. *Biochim. Biophys. Acta* **2004**, *1655*, 116−122.

(7) Martinez-Rivera, M. C.; Berry, B. W.; Valentine, K. G.; Westerlund, K.; Hay, S.; Tommos, C. Electrochemical and Structural Properties of a Protein System Designed to Generate Tyrosine Pourbaix Diagrams. *J. Am. Chem. Soc.* **2011**, *133*, 17786−17795.

(8) Berry, B. W.; Martinez-Rivera, M. C.; Tommos, C. Reversible Voltammograms and a Pourbaix Diagram for a Protein Tyrosine Radical. *Proc. Natl. Acad. Sci. U.S.A.* **2012**, *109*, 9739−9743.

(9) Bensasson, R. V.; Land, E. J.; Truscott, T. G. *Pulse Radiolysis and Flash Photolysis: Contributions to the Chemistry of Biology and Medicine*; Pergamon Press Ltd.: Oxford, U.K., 1983.

(10) Ignasiak, M.; Scuderi, D.; de Oliveira, P.; Pedzinski, T.; Rayah, Y.; Houee Levin, C. Characterization by Mass Spectrometry and IRMPD Spectroscopy of the Sulfoxide Group in Oxidized Methionine and Related Compounds. *Chem. Phys. Lett.* **2011**, *502*, 29−36.

(11) Fourré, I.; Bergès, J. Structural Properties and Topological Characterization of the Three-Electron Bond: the SO Radicals. *J. Phys. Chem. A* **2004**, *108*, 898−906.

(12) Bobrowski, K.; Schoneich, C.; Holcman, J.; Asmus, K. D. OH Radical Induced Decarboxylation of γ-Glutamylmethionine and S-Alkylglutathione Derivatives: Evidence for Two Different Pathways Involving C- and N-Terminal Decarboxylation. *J. Chem. Soc., Perkin Trans. 2* **1991**, 353−362.

(13) Bobrowski, K.; Schoneich, C. Decarboxylation Mechanism of the N-Terminal Glutamyl Moiety in γ-Glutamic Acid and Methionine Containing Peptides. *Radiat. Phys. Chem.* **1996**, *47*, 507−510.

(14) Bobrowski, K.; Houée-Levin, C.; Marciniak, B. Stabilization and Reactions of Sulfur Radical Cations: Relevance to One-Electron Oxidation of Methionine in Peptides and Proteins. *Chimia* **2008**, *62*, 728−734.

(15) Grune, T.; Jung, T.; Merker, K.; Davies, K. J. Decreased Proteolysis Caused by Protein Aggregates, Inclusion Bodies, Plaques, Lipofuscin, Ceroid, and 'Aggresomes' during Oxidative Stress, Aging, and Disease. *Int. J. Biochem. Cell Biol.* **2004**, *36*, 2519−2530.

(16) Mozziconacci, O.; Mirkowski, J.; Rusconi, F.; Pernot, P.; Bobrowski, K.; Houee-Levin, C. Superoxide Radical Anions Protect Enkephalin from Oxidation If the Amine Group Is Blocked. *Free Radical Biol. Med.* **2007**, *43*, 229−234.

(17) Mozziconacci, O.; Mirkowski, J.; Rusconi, F.; Kciuk, G.; Wisniowski, P.; Bobrowski, K.; Houée-Levin, C. Methionine Residue Acts as a Prooxidant in the ·OH-Induced Oxidation of Enkephalins. *J. Phys. Chem. B* **2012**, *116*, 9352−9362.

(18) Ignasiak, M. T.; de Oliveira, P.; Houée Levin, C.; Scuderi, D. Oxidation of Methionine-Containing Peptides by OH Radicals: Is Sulfoxide the Only Product? Study by Mass Spectrometry and IRMPD Spectroscopy. *Chem. Phys. Lett.* **2013**, *590*, 35−40.

(19) Bergès, J.; Trouillas, P.; Houée-Levin, C. Oxidation of Protein Tyrosine or Methionine Residues: From the Amino Acid to the Peptide. *J. Phys. Conf. Ser.* **2011**, *261*, 012003.

(20) Trouillas, P.; Bergès, J.; Houée-Levin, C. Towards Understanding the Protein Oxidation Processes. OH Addition on Tyrosine, Phenylalanine or Methionine. *Int. J. Quantum Chem.* **2011**, *111*, 143−151.

(21) Marcotte, I.; Separovic, F.; Auger, M.; Gagne, S. M. A Multidimensional ^{1}H NMR Investigation of the Conformation of Methionine-Enkephalin in Fast-Tumbling Bicelles. *Biophys. J.* **2004**, *86*, 1587−1600.

(22) Vengadesan, K.; Anbupalam, T.; Gautham, N. An Application of Experimental Design Using Mutually Orthogonal Latin Squares in Conformational Studies of Peptides. *Biopolymers* **2004**, *74*, 476−494.

(23) Hansmann, U. H.; Okamoto, Y.; Onuchic, J. N. The Folding Funnel Landscape for the Peptide Met-Enkephalin. *Proteins* **1999**, *34*, 472−483.

(24) Ramya, L.; Gautham, N. Conformational Space Exploration of Met- and Leu-Enkephalin Using the MOLS Method, Molecular Dynamics, and Monte Carlo Simulation—A Comparative Study. *Biopolymers* **2012**, *97*, 165−176.

(25) Petruk, A. A.; Bartesaghi, S.; Trujillo, M.; Estrin, D. A.; Murgida, D.; Kalyanaraman, B.; Marti, M. A.; Radi, R. Molecular Basis of Intramolecular Electron Transfer in Proteins during Radical-Mediated Oxidations: Computer Simulation Studies in Model Tyrosine−Cysteine Peptides in Solution. *Arch. Biochem. Biophys.* **2012**, *525*, 82−91.

(26) Pilmé, J.; Luppi, E.; Bergès, J.; Houée Levin, C.; de la Lande, A. Topological Analyses of Time-Dependent Electronic Structures: Application to Electron-Transfers in Methionine Enkephalin. *J. Mol. Model.* **2014**, *20*, 2368.

(27) Frisch, M. J.; Trucks, G. W.; Schlegel, H. B.; Scuseria, G. E.; Robb, M. A.; Cheeseman, J. R.; Scalmani, G.; Barone, V.; Mennucci, B.; Petersson, G. A.; et al. *Gaussian 09*; Gaussian Inc.: Wallingford, CT, 2009.

(28) Bergès, J.; de Oliveira, P.; Fourré, I.; Houée Levin, C. The One-Electron Reduction Potential of Methionine-Containing Peptides Depends on the Sequence. *J. Phys. Chem. B* **2012**, *116*, 9352−9362.

(29) Liptak, M. D.; Shields, G. C. Accurate pK_a Calculations for Carboxylic Acids Using Complete Basis Set and Gaussian-n Models Combined with CPCM Continuum Solvation Methods. *J. Am. Chem. Soc.* **2001**, *123*, 7314−7319.

(30) Rickard, G. A.; Bergès, J.; Houée Levin, C.; Rauk, A. Ab Initio and QM/MM Study of Electron Addition on the Disulfide Bond in Thioredoxin. *J. Phys. Chem. B* **2008**, *112*, 5774−5787.

(31) Silvi, B.; Savin, A. Classification of Chemical Bonds Based on Topological Analysis of Electron Localization Functions. *Nature* **1994**, *371*, 683−686.

(32) Bader, R. E. *Atoms in Molecules: A Quantum Theory*; Oxford University Press: Oxford, U.K., 1994.

(33) Becke, A. D.; Edgecombe, K. E. A Simple Measure of Electron Localization in Atomic and Molecular Systems. *J. Chem. Phys.* **1990**, *92*, 5397−5403.

(34) Burnus, T.; Marques, M. A. L.; Gross, E. K. U. Time-dependent Electron Localization Function. *Phys. Rev. A* **2005**, *71*, 010501−010504.

(35) Kaduk, B.; Kowalczyk, T.; Van Voorhis, T. Constrained Density Functional Theory. *Chem. Rev.* **2012**, *112*, 321−370.

(36) Köster, A. M.; Calaminici, P.; Casida, M. E.; Dominguez, V. D.; Flores-Moreno, R.; Geudtner, G.; Goursot, A.; Heine, Th.; Ipatov, A.; Janetzko, F.; Del Campo, J. M.; Reveles, J. U.; Vela, A.; Zuniga, B.; Salahub, D. R. *deMon2k*, version 2; The deMon developers, 2006.

(37) Jovanovic, S. V.; Harriman, A.; Simic, M. G. Electron Transfer Reactions of Tryptophan and Tyrosine Derivatives. *J. Phys. Chem.* **1986**, *90*, 1935−1940.

(38) Folkes, L. K.; Trujillo, M.; Bartesaghi, S.; Radi, R.; Wardman, P. Kinetics of Reduction of Tyrosine Phenoxyl Radicals by Glutathione. *Arch. Biochem. Biophys.* **2011**, *506*, 242−249.

(39) Harriman, A. Further Comments on the Redox Potentials of Tryptophan and Tyrosine. *J. Phys. Chem.* **1987**, *91*, 6102−6104.

(40) DeFelippis, M. R.; Murthy, C. P.; Faraggi, M.; Klapper, M. H. Pulse Radiolytic Measurement of Redox Potentials: The Tyrosine and Tryptophan Radicals. *Biochemistry* **1989**, *28*, 4847−4853.